

# Optical forces from evanescent Bessel beams, multiple reflections and Kerker conditions in magnetodielectric spheres and cylinders

Juan Miguel Auñón<sup>1,\*</sup> and Manuel Nieto-Vesperinas<sup>1</sup>

<sup>1</sup>*Instituto de Ciencia de Materiales de Madrid, Consejo Superior de Investigaciones Científicas, Campus de Cantoblanco, Madrid 28049, Spain.*

In this work we address, first, the optical force on a magnetodielectric particle on a flat dielectric surface due to an evanescent Bessel beam and, second, the effects on the force of multiple scattering with the substrate. For the first question we find analytical solutions showing that due to the interference of the excited electric and magnetic particle dipoles, the vertical force unusually pushes the object out from the plane. The incident wavelength rules whether the illumination constitutes, or not, an optical trap. As for the second problem, we make a 2D study with a single evanescent plane wave, and we present the Kerker conditions, (so far established for spheres), for magnetodielectric cylinders; showing that in  $p$ -polarization those are practically reproduced and are associated to minima of the horizontal and vertical forces.

## I. INTRODUCTION

In the area of near-field optics and nanophotonics the role of evanescent waves is crucial. In the most simple configuration, namely that of total internal reflection (TIR) beyond a critical incidence angle  $\theta_c$ , there have been several studies on the mechanical action of evanescent waves on micro and nanoparticles in order to create traps and manipulate them in several ways [1–6]. This question has acquired a renewed interest after the discovery of tractor beams [7–10] capable of pulling particles by negative radiation pressure (NRP) as a consequence of the interference of electric and magnetic dipoles when both are resonantly excited in such bodies [11, 12]. However, in spite of the interest of optical manipulation of particles with subwavelength resolution [13], to date no detailed theory nor controlled experiments exist on the possibilities of both trapping and creating tractor evanescent waves either by TIR or by excitation of surface plasmon polaritons (SPP) at flat surfaces of noble metals [14]. Only some detailed calculations [15, 16] report on this problem, although the particles addressed have a low refractive index and thus no strong magnetodielectric resonances.

To tackle this question, in this paper we carry out a theoretical and numerical study on the optical forces exerted on a dielectric particle with magnetic response on a flat dielectric surface under TIR conditions. Such kind of objects have triggered much interest due to their inherent optical magnetism [17–21]. Propagating Bessel beams [22, 23] have manifested as suitable for creating NRP on these bodies in absence of surfaces [7, 8, 10]. Nevertheless, as far as we know their mechanical response to evanescent Bessel fields in TIR or SPP configurations have never been discussed. This problem goes beyond the study initiated in [14] for non-resonant magnetic parti-

cles since it has two sides: on the one hand, the scattering of an incident evanescent Bessel beam on a resonant magnetodielectric particle placed on a dielectric plane at which TIR occurs, and on which no multiple interactions take place. On the other hand, evanescent fields convey interfaces at which they are created; hence if these are close to a particle with a rather large scattering cross section, which may occur at peak excitation of its electric and / or magnetic resonant modes, such multiple reflections and scatterings will unavoidably be present, and we do not know detailed studies where their effect on the photonic forces have been addressed.

Therefore, we shall first present in Section II an analysis (to be referred to as AR) of the forces upon a Si sphere in air with magnetodielectric response to illumination, exerted by an evanescent Bessel beam transmitted from a dielectric plane by TIR. This will ignore multiple scattering with the plane. However, in contrast with previous studies on the action of evanescent waves on non-resonant objects, it will be shown in Section III how at resonant wavelengths, and depending on the signs and relative phases of polarizabilities, evanescent Bessel beams can exert repulsive vertical forces on magnetodielectric bodies. This latter effect will be shown to be assisted by the plane which gives rise to the above mentioned multiple reflections.

Indeed the electric and magnetic dipole modes excited on the particle, (characterized by its first electric and magnetic Mie resonances, respectively), involve large scattering cross sections under resonant illumination and hence such multiple scattering in many real situations. However, this analysis (to be denoted as MR) will be done with 2D numerical computations on an infinite cylinder, rather than with a sphere. Also, a single evanescent plane wave, rather than a Bessel beam, will be assumed to illuminate the object.

We reason that 2D results should translate to 3D configurations because of the small differences existing between scattering from magnetodielectric spheres and cylinders under  $p$ -polarization, (i.e. with the incident

\* Corresponding author: jmaunon@icmm.csic.es

electric vector in the plane of incidence). To this end we shall present details never discussed so far on electromagnetic scattering in magnetodielectric cylinders, showing, like in spheres [24], suppression of the scattered radiation in either the backward or forward directions. The consequences of these effects on the optical forces will also be discussed.

## II. OPTICAL FORCES FROM EVANESCENT BESSEL BEAMS

Bessel beams are non-diffracting solutions of the homogeneous Helmholtz equation [22, 23]. In the scalar formulation, their wavefunction is  $U(r, \phi, z) = J_0(qr) e^{im\phi} e^{i\beta'z}$ , with  $\beta'^2 = k^2 - q^2$ ;  $k = nk_0$ ,  $k_0 = 2\pi/\lambda$  and  $n$  is the refractive index of the medium.  $q$  and  $\beta'$  denote the transversal and longitudinal components of the wavevector, respectively. If  $q^2 > k^2$ ,  $\beta'$  becomes imaginary and the wave amplitude decays along the  $z$ -direction. Here we shall consider the electric and magnetic vectors of evanescent Bessel beams created by TIR on a dielectric plane  $z = 0$ . We employ cylindrical coordinates  $(r, \phi, z)$ , so that the beam axis is directed along  $OZ$  and  $\beta' = i\beta = i\sqrt{q^2 - k^2}$  [25, 26]. Assuming harmonic time dependence,  $\exp(-i\omega t)$ , these vectors are:

$$\mathbf{E}(\mathbf{r}) = e^{im\phi - \beta z} (E_r \hat{\mathbf{e}}_r + E_\phi \hat{\mathbf{e}}_\phi + E_z \hat{\mathbf{e}}_z), \quad (1)$$

$$\mathbf{H}(\mathbf{r}) = e^{im\phi - \beta z} (H_r \hat{\mathbf{e}}_r + H_\phi \hat{\mathbf{e}}_\phi + H_z \hat{\mathbf{e}}_z), \quad (2)$$

where  $E_i$  and  $H_i$  ( $i = r, \phi, z$ ) are

$$E_r = -\frac{\beta}{q} c_2 J'_m(qr) - \frac{km}{q^2 r} c_1 J_m(qr), \quad (3)$$

$$E_\phi = -\frac{ik}{q} c_1 J'_m(qr) - \frac{i\beta m}{q^2 r} c_2 J_m(qr), \quad (4)$$

$$E_z = J_m(qr) c_2, \quad (5)$$

and

$$H_r = -\frac{\beta}{q} c_1 J'_m(qr) + \frac{km}{q^2 r} c_2 J_m(qr), \quad (6)$$

$$H_\phi = \frac{ik}{q} c_2 J'_m(qr) - \frac{i\beta m}{q^2 r} c_1 J_m(qr), \quad (7)$$

$$H_z = J_m(qr) c_1. \quad (8)$$

In these equations  $J_m(qr)$  is the Bessel function of order  $m$ , ( $m = 0, 1, 2, \dots$ ),  $J'_m(qr) = dJ_m/dqr$ , and the arbitrary complex coefficients  $c_1$  and  $c_2$  describe the amplitude and the phase of TE ( $s$ ) and TM ( $p$ ) polarized waves, respectively.

Now we address the electromagnetic force from such an evanescent Bessel beam on interaction with a magnetodielectric particle. For dipolar particles, i.e. those whose scattering properties are fully characterized by their induced electric and magnetic dipoles [12, 19, 27], this force  $\mathbf{F}$  is the sum:  $\mathbf{F} = \mathbf{F}^e + \mathbf{F}^m + \mathbf{F}^{em}$  on the excited electric dipole:  $\mathbf{F}^e$ , magnetic dipole:  $\mathbf{F}^m$  and interference

between them:  $\mathbf{F}^{em}$ . It can be obtained substituting Eqs. (3)-(8) into Eqs. (42)-(44) of reference [11]. Assuming that the particle is in vacuum, the expressions for these electric, magnetic and interference forces along the radial coordinate are:

$$\begin{aligned} F_r^e &= \frac{1}{2} \text{Re} \{ \alpha_e^s \mathbf{E} \partial_r \mathbf{E}^* \} \\ &= \frac{1}{2} \text{Re} \{ \alpha_e^s \} e^{-2\beta z} \left( \frac{1}{8q} \left[ (k^2 |c_1|^2 + \beta^2 |c_2|^2) \right. \right. \\ &\quad \times \left( \frac{2m J_m}{qr} (J_{m-2} - J_{m+2}) + 4J'_m (J'_{m-1} - J'_{m+1}) \right) \\ &\quad \left. \left. + k\beta \text{Re} \{ c_1 c_2^* \} \left( \frac{4m J_m}{qr} (J_{m-1} - J_{m+1}) \right. \right. \right. \\ &\quad \left. \left. \left. + 2J'_m (J_{m-2} - J_{m+2}) \right) \right] + |c_2|^2 q J_m J'_m \right), \end{aligned} \quad (9)$$

$$\begin{aligned} F_r^m &= \frac{1}{2} \text{Re} \{ \alpha_m^s \mathbf{H} \partial_r \mathbf{H}^* \} \\ &= \frac{1}{2} \text{Re} \{ \alpha_m^s \} e^{-2\beta z} \left( \frac{1}{8q} \left[ (k^2 |c_2|^2 + \beta^2 |c_1|^2) \right. \right. \\ &\quad \times \left( \frac{2m J_m}{qr} (J_{m-2} - J_{m+2}) + 4J'_m (J'_{m-1} - J'_{m+1}) \right) \\ &\quad \left. \left. - k\beta \text{Re} \{ c_1 c_2^* \} \left( \frac{4m J_m}{qr} (J_{m-1} - J_{m+1}) \right. \right. \right. \\ &\quad \left. \left. \left. + 2J'_m (J_{m-2} - J_{m+2}) \right) \right] + |c_1|^2 q J_m J'_m \right), \end{aligned} \quad (10)$$

$$\begin{aligned} F_r^{em} &= -\frac{k^4}{3} [\text{Re} \{ \alpha_e^s \alpha_m^{s*} \} \text{Re} (\mathbf{E} \times \mathbf{H}^*)_r \\ &\quad - \text{Im} \{ \alpha_e^s \alpha_m^{s*} \} \text{Im} (\mathbf{E} \times \mathbf{H}^*)_r] \\ &= -\frac{k^4}{3} \left[ -\frac{2\beta m}{q^2 r} J_m^2 \text{Re} \{ \alpha_e^s \alpha_m^{s*} \} \text{Im} \{ c_1 c_2^* \} + \text{Im} \{ \alpha_e^s \alpha_m^{s*} \} \right. \\ &\quad \left. \times \left( \frac{k}{q} J_m J'_m (|c_2|^2 - |c_1|^2) + \frac{\beta m}{q^2 r} J_m^2 \text{Re} \{ c_1 c_2^* \} \right) \right]. \end{aligned} \quad (11)$$

If the particle is dipolar in the wide sense [12, 19], its magnetodielectric response, assumed it spherical, is characterized by its electric and magnetic polarizabilities

$$\alpha_e^s = i \frac{3}{2k^3} a_1^s, \quad \alpha_m^s = i \frac{3}{2k^3} b_1^s, \quad (12)$$

$a_1^s$  and  $b_1^s$  standing for the electric and magnetic first Mie coefficients [28]. The superscript  $s$  denotes that these quantities correspond to a sphere. For this type of illumination Eqs. (9)-(10) show that these radial components of the force are purely conservative (i.e. they are gradient forces) because the imaginary part of  $\alpha_e^s$  or  $\alpha_m^s$  does not contribute [11, 29]. Nevertheless Eq. (11) describes a non-conservative component associated to the electromagnetic interference force given by the product of these polarizabilities.

Likewise we obtain the force along the azimuthal  $\hat{\mathbf{e}}_\phi$  direction:

$$\begin{aligned} F_\phi &= F_\phi^e + F_\phi^m + F_\phi^{em} \\ &= \frac{1}{2} \text{Im}\{\alpha_e^s\} \frac{m |\mathbf{E}|^2}{r} + \frac{1}{2} \text{Im}\{\alpha_m^s\} \frac{m |\mathbf{H}|^2}{r} \\ &\quad - \frac{k^4}{3} \text{Re}\{\alpha_e^s \alpha_m^{s*}\} \frac{km}{q^2 r} J_m^2(qr) (|c_1|^2 + |c_2|^2). \end{aligned} \quad (13)$$

Where

$$\begin{aligned} |\mathbf{E}|^2 / e^{-2\beta z} &= \left( k^2 |c_2|^2 + \beta^2 |c_2|^2 \right) \left( \frac{J_m'^2(qr)}{q^2} + \frac{m^2 J_m^2(qr)}{q^4 r^2} \right) \\ &\quad + |c_2|^2 J_m^2(qr) + \frac{4k\beta m}{q^3 r} J_m'(qr) J_m(qr) \text{Re}\{c_1 c_2^*\} \end{aligned} \quad (14)$$

$$\begin{aligned} |\mathbf{H}|^2 / e^{-2\beta z} &= \left( k^2 |c_2|^2 + \beta^2 |c_1|^2 \right) \left( \frac{J_m'^2(qr)}{q^2} + \frac{m^2 J_m^2(qr)}{q^4 r^2} \right) \\ &\quad + |c_1|^2 J_m^2(qr) - \frac{4k\beta m}{q^3 r} J_m'(qr) J_m(qr) \text{Re}\{c_1 c_2^*\} \end{aligned} \quad (15)$$

The first two terms of Eq. (13) are non-conservative and push the particle towards the positive azimuthal direction. The third term due to the interference of the electric and magnetic dipoles is either positive or negative depending on the sign of  $\text{Re}\{\alpha_e^s \alpha_m^{s*}\}$ . It is worth remarking that Eq. (13) is analogous to Eq. (2) of [8] in the sense that this azimuthal force will be negative if the third term of Eq. (13) dominates over the first two. This is a new situation that deserves a discussion.

The most favorable situation to achieve such a negative azimuthal force is when  $\alpha_e^s = \alpha_m^s$  [10], this corresponds to  $a_1^s = b_1^s$ , which pertains to the well-known *first Kerker's condition* [24] to be further discussed in Section III. In this case, and using the optical theorem for non-absorbing particles [19], one has that:  $\text{Im}\alpha_e^s = 2k^3 |\alpha_e^s|^2 / 3$ . However, even including this latter case, it is easy to see from Eq.(12) that  $F_\phi > 0$  for any polarization, wavelength, or order  $m$ . Thus *the azimuthal force from an evanescent Bessel beam is always positive*; at least as long as there be no multiple scattering with the substrate interface.

On the other hand, the force components in the  $z$ -direction are:

$$F_z^e = \frac{-\beta}{2} \text{Re}\{\alpha_e^s\} |\mathbf{E}|^2, \quad F_z^m = \frac{-\beta}{2} \text{Re}\{\alpha_m^s\} |\mathbf{H}|^2, \quad (16)$$

$$\begin{aligned} F_z^{em} &= -\frac{k^4}{3} [\text{Re}\{\alpha_e^s \alpha_m^{s*}\} \text{Re}(\mathbf{E} \times \mathbf{H}^*)_z \\ &\quad - \text{Im}\{\alpha_e^s \alpha_m^{s*}\} \text{Im}(\mathbf{E} \times \mathbf{H}^*)_z] = \\ &= -\frac{k^4}{3} e^{-2\beta z} \left[ -\text{Re}\{\alpha_e^s \alpha_m^{s*}\} J_m J_m' \frac{2m}{q^3 r} (k^2 - \beta^2) \text{Im}\{c_1 c_2^*\} \right. \\ &\quad - \text{Im}\{\alpha_e^s \alpha_m^{s*}\} \left( \left( \frac{k\beta}{q^2} J_m'^2 + \frac{k\beta m^2}{q^4 r^2} J_m^2 \right) (|c_2|^2 - |c_1|^2) \right. \\ &\quad \left. \left. + J_m J_m' \frac{2m}{q^3 r} (k^2 - \beta^2) \text{Re}\{c_1 c_2^*\} \right) \right]. \end{aligned} \quad (17)$$

Since the intensity  $|\mathbf{E}|^2$  decays along the  $z$ -direction as  $\exp(-2\beta z)$ , there is a gradient force, one for the electric dipole and one for the magnetic, which will attract or repel the particle with respect to the plane  $z = 0$  depending on whether the real part of the corresponding polarizability is positive or negative. Notice also from Eqs. (11), (13) and (17) that the non-conservative component  $F_z^{em}$  due to the interference between both dipoles is zero if and only if  $|c_2|^2 = |c_1|^2$  and  $m = 0$ ; (compare with the total azimuthal force  $F_\phi$  which is zero for  $m = 0$ ).

In order to illustrate these results, let us consider a magnetodielectric sphere of Si illuminated in the near infrared [19], its refractive index being  $n_p \simeq \sqrt{12}$ . In the range of size parameter  $n_p k r_0 < 4.2$ , ( $r_0$  being the radius of the sphere), it behaves as dipolar in the wide sense [12].

Figs. 1 and 2 illustrate the non-zero components of the force from a Bessel beam with  $m = 0$ , ( $c_1 = 1$ ,  $c_2 = i$ ,  $q/k = 2$ ), and  $m = 1$ , ( $c_1 = 1$ ,  $c_2 = i$ ,  $q/k = 2.0$ ), respectively, for three values of  $\lambda$  and for a Si sphere of  $r_0 = 230 \text{ nm}$ . As shown above, all the interference and azimuthal forces are zero for  $m = 0$ ; also in this case Eqs. (9)-(10) and (16), show that the total force will be negative when both  $\text{Re}\{\alpha_e^s\}$  and  $\text{Re}\{\alpha_m^s\}$  are positive, [cf. Fig. 3 (a)]; then  $F_r$  will pull the particle towards  $r = 0$ , and  $F_z$  will act as tractor force also pulling it towards the plane  $z = 0$ .

The case  $m = 1$  presents a richer behavior since now the non-conservative  $F_r^{em}$  and  $F_z^{em}$  components compete with those from the pure dipoles and can overcome them depending on the polarizabilities. In this respect it is interesting to see in Fig. 2 that while the purely electric and magnetic  $r$  and  $z$ -components of the force from the Bessel beam evanescent along  $OZ$ , are gradient and hence conservative forces, (and for  $F_z$  this is in contrast with a Bessel beam propagating in the  $z$ -direction which induces a scattering and thus no conservative force in this direction [8]), at certain values of the polarizabilities [cf. Fig. 3 (a)]  $F_r^{em}$  and  $F_z^{em}$  become attractive towards the center of the beam and the plane, respectively, thus contributing to a resulting trapping force. Therefore, *tailoring the electric and magnetic polarizabilities* [according to Fig. 3 (a)] *the particle will, or will not, be trapped, depending on the signs and relative phases of the polarizabilities at the illuminating wavelength*. Trapping is clearly seen in Figs. 1 and 2 for  $\lambda = 1.75 \mu\text{m}$ . Notice that actually the radial component of the force is similar to that from a

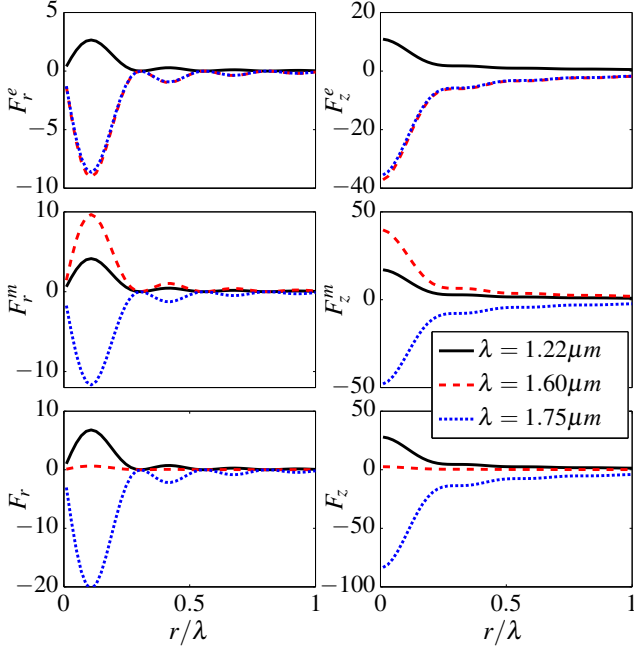


FIG. 1. Optical force components, in arbitrary units, normalized to  $\exp(-2\beta z)$  on a Si sphere of  $r_0 = 230\text{nm}$  from an evanescent Bessel beam with  $m = 0$ . The horizontal rows show the electric and magnetic forces and the sum of both respectively (the interference components  $F_r^{em}$  and  $F_z^{em}$  are zero).

propagating Bessel beam [8] since the  $r$  dependence is the same.

Conversely, we observe in Fig. 2 wavelengths where  $F_z^{em}$  is opposite to the force from a pure dipole, (we recall that the sign of  $\mathbf{F}^{em}$  depends on the relative phases of  $\alpha_e^s$  and  $\alpha_m^s$ ), and thus this interference component may contribute to changing the sign of the total vertical force. For example, at  $\lambda = 1.60\mu\text{m}$   $F_z^{em}$  opposes to the attractive  $F_z^e$ , and together with  $F_z^m$  produces a repulsive total vertical component  $F_z$  even though the Bessel beam is evanescent along  $OZ$ . This is a consequence of the particle magnetodielectric resonant behavior and constitutes a novel situation opposite to those studied before [1, 2, 30] with evanescent plane waves that produce attractive vertical forces on passive non-resonant particles.

### III. OPTICAL FORCES IN PRESENCE OF MULTIPLE REFLECTIONS

So far we have not addressed the interaction of the evanescent beam with the surface that created it. This is an approach of frequent use in the literature. However, the existence of interfaces, inherent to such illuminating configurations, should introduce multiple scattering of the waves with the objects and the surfaces over which they are placed [15]. This should be even more prevalent

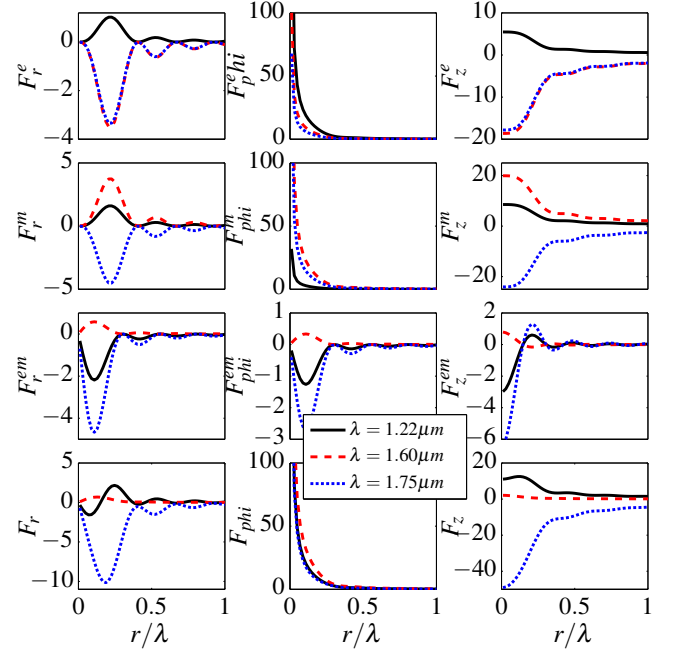


FIG. 2. The same as Fig. 1 when  $m = 1$ . The horizontal rows show the electric, magnetic, interference and the total force for each component, respectively.

under particle resonance conditions here studied, since then its scattering cross-section is larger, thus giving rise to multiple reflections of the field with the interface. This imposes a comparison of the ideal incident illumination model studied above, with that taking into account such multiple scattering.

Without loss of generality, we now carry on numerical simulations in order to tackle this problem. The main goal is to check the range of validity of the non-multiple scattering model for such large resonant particles as those with magnetodielectric response considered in this work. To make this task simpler, we consider only one plane wave component of the incident beam, which gives rise under TIR to one evanescent component of the non-radiating beam transmitted at  $z = 0$  and illuminating the particle. This reasoning is warranted by the fact that the incident beam suffering TIR at  $z = 0$  and generating an evanescent beam, is a superposition of plane waves, expressed by the angular spectrum representation of its wavefield. Since the evanescent beam is characterized by a small angular dispersion of such non-radiating plane wave components [31, 32], the deviations, or their absence, between the results for a single plane wave component neglecting the field multiple reflections and those addressing them, would automatically be translated to the beam as it is built by superposing all such plane waves.

Also, since full 3D computational simulations are numerically expensive, we deal with the problem using 2D

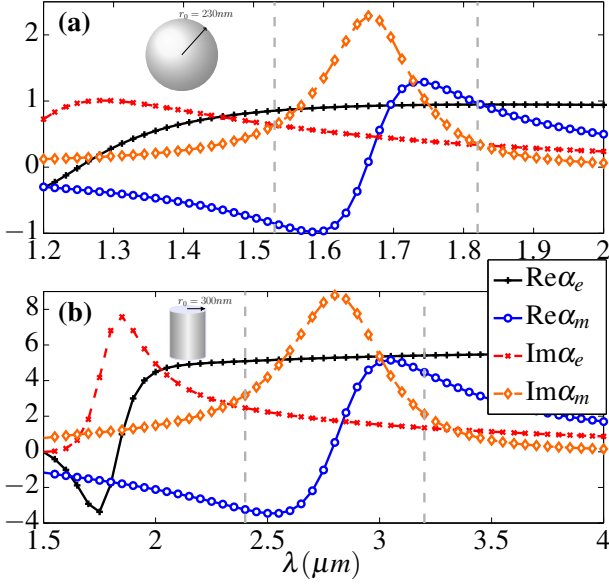


FIG. 3. Real and imaginary parts of the electric ( $\alpha_e$ ) and magnetic ( $\alpha_m$ ) polarizabilities. (a) Sphere of radius  $r_0 = 230\text{nm}$  (cf. Fig. 1(a) of [19]). (b) Cylinder of radius  $r_0 = 300\text{nm}$ . A plane polarized plane wave incides on the particles. The results are normalized to  $r_0^3$  for the sphere and to  $r_0^2$  for the cylinder. The vertical broken lines indicate the 1st (right) and 2nd (left) Kerker condition wavelengths.

calculations, therefore we have chosen cylinders instead of spheres. In this connection notice that if one addresses multiply reflected Bessel beams, a full 3D calculation with a sphere should be done.

#### A. Scattering properties of magnetodielectric cylinders

Prior to entering in details of multiple reflection effects, we discuss some scattering properties, never studied before, of an infinitely long magnetodielectric dipolar cylinder illuminated by a plane polarized plane wave with incidence normal to the cylinder axis, comparing them with those of a sphere [12, 19]. This is a case much less addressed than that of a spherical particle.

The electric and magnetic polarizabilities of an infinite cylinder under  $p$ -polarization, i.e. with its axis along the  $\mathbf{H}$ -field and perpendicular to the incident wavevector, are (notice now the superscript  $c$ ):

$$\alpha_e^c = i \frac{2}{\pi k^2} a_1, \quad \alpha_m^c = i \frac{1}{\pi k^2} a_0 \quad (18)$$

Details of these latter expressions can be found in the Appendix.  $p$ -polarization is the one under which the spectral behavior of the polarizabilities of the cylinder are very similar to those of a sphere. A comparison between the polarizabilities of a Silicon sphere of radius

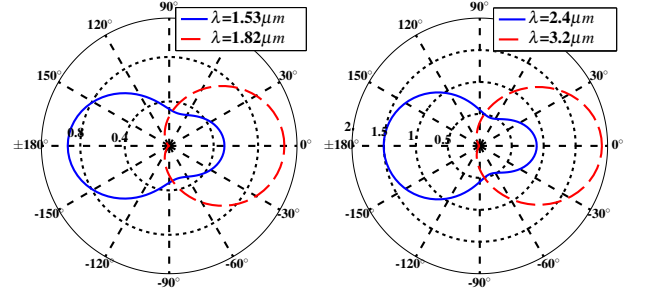


FIG. 4. Angular distribution of intensity scattered from a magnetodielectric dipolar sphere (left) and cylinder under  $p$ -polarized illumination (right). The solid lines (blue) depict the intensities at the wavelengths under which they become zero (sphere) or near zero (cylinder) in  $\theta = 0$ , whereas the dashed (red, which appear multiplied by 1.52) lines plot the intensities at the wavelengths at which they are near zero in  $\theta = \pi$  both for the sphere and cylinder.

$r_0 = 230\text{nm}$  and cylinder with  $r_0 = 300\text{nm}$  is seen in Figs. 3 (a) and (b), respectively. [The results of Fig. 3(a) were obtained in [19] and are given here to facilitate comparison with those of Fig. 3(b)].

In addition, the angular distribution of scattered intensity for magnetodielectric spheres and cylinders are [20, 28]:

$$I^s(\theta) \propto |a_1^s \cos \theta + b_1^s|^2, \quad I^c(\theta) \propto |a_0^c + 2a_1^c \cos \theta|^2, \quad (19)$$

respectively. The Mie coefficients  $a_n^s, b_n^s, a_n^c$  can be found in e.g. [28]. Using Eqs. (12) and (18) the intensities can be written in terms of the polarizabilities and calculated from the values of Figs. 3 (a) and (b).

Two interesting scattering angles are those of the forward ( $\theta = 0$ ) and backward ( $\theta = \pi$ ) directions.

In forward scattering, the angular intensity is minimum if  $\text{Re}\alpha_e^{s,c} = -\text{Re}\alpha_m^{s,c}$ ,  $\text{Im}\alpha_e^{s,c} = \text{Im}\alpha_m^{s,c}$ , (for spheres see [19, 20, 24]). From Fig. 3 one can see that the *minimum forward intensity* is given at  $\lambda \simeq 1.53\mu\text{m}$  (second Kerker condition) for the sphere and at  $\lambda \simeq 2.4\mu\text{m}$  for the cylinder.

In the backward direction,  $\theta = \pi$ , the intensity is zero if  $a_1^s = b_1^s$  (i.e.  $\text{Re}\alpha_e^s = \text{Re}\alpha_m^s$ ,  $\text{Im}\alpha_e^s = \text{Im}\alpha_m^s$ ) for spheres, (first Kerker condition), [19, 20, 24], or if  $a_0^c = 2a_1^c$ , ( $\text{Re}\alpha_m^c = \text{Re}\alpha_e^c$ ,  $\text{Im}\alpha_m^c = \text{Im}\alpha_e^c$ ) for cylinders. For the sphere this latter condition is obtained at  $\lambda \simeq 1.82\mu\text{m}$ , being  $I^s(\theta)$  exactly zero. However, due to the factor 2 of the  $a_1^c$  term in  $I^c(\theta)$ , [cf. the second Eq. (19)], such a zero backward intensity cannot be created by an infinitely long dipolar cylinder; nevertheless it can be minimum and close to zero. In our example this happens at  $\lambda = 3.2\mu\text{m}$ .

Fig. 4 depicts the angular scattered intensities for the above quoted wavelengths, demonstrating that these aforementioned anomalous scattering properties of magnetodielectric spheres at  $\theta = \pi$  and  $\theta = 0$  are almost

reproduced in magnetodielectric infinite cylinders under  $p$ -polarization.

### B. Effects of multiple reflections

Based on the above discussed similarities of the scattering from dipolar spheres and cylinders under  $p$ -polarization, we consider a propagating plane wave whose electric field amplitude per sectional plane  $y = 0$  of the cylinder is  $1V/m$ , impinging at an angle  $\theta_0 = 34.2^\circ > \theta_c$  into the plane interface  $z = 0$  that separates a dielectric of refractive index  $n_1 = 2.58$  from air. We study its scattering with a magnetodielectric cylinder of radius  $r_0$  placed in the air at different distances  $d$  from the plane, (i.e. with axis at  $z = d + r_0$ ,  $n_p = \sqrt{12}$  and  $r_0 = 300nm$ ).

In order to compare full numerical calculations of multiple reflection calculations (MR) with analytical results (AR) of an incident evanescent wave that ideally does not suffer multiple scattering with the  $z = 0$  plane, we first obtain the electromagnetic force  $\mathbf{F}$  on the cylinder by means of Maxwell's stress tensor (MST)  $\mathbf{T}$ , i.e.,  $\mathbf{F} = \int \mathbf{T} \mathbf{n} dS$ ,  $\mathbf{n}$  being the unit outward normal to an arbitrary surface  $S$  which encloses the particle [33]. Notice that the fields from which the MST is obtained are total, i.e. incident plus scattered:  $\mathbf{E}_i + \mathbf{E}_s$  and  $\mathbf{H}_i + \mathbf{H}_s$ .

The MR so obtained are exact within the resolution provided by the numerical procedure. This is a finite element method (FEM), (RF module of Comsol 4.3). Details of how to calculate optical forces with the MST in a Comsol platform are to reported in [34]. Several grid samplings are done in order to check convergence of the computations. We then compare these MR calculations with the AR obtained from an evanescent plane wave [14] that arises on transmission at  $z = 0$  of the same  $p$ -polarized plane wave propagating in the dielectric side. (We correct misprints of Eqs. (2), (5) and (6) of [14] for the horizontal and vertical components of  $\mathbf{F}^e$  and  $\mathbf{F}^{em}$ . The right side of (2) must be multiplied by  $-1$ . The factor  $2\frac{K^2}{k^2} - 1$  should be replaced by  $1$  in (5) and by  $-1$  in (6). Notice that from those equations one has:  $F_x = F_x^e + F_x^m + F_x^{em} \geq 0$ .)

Fig. 5 shows the total force  $\mathbf{F}(\mathbf{r}) = \mathbf{F}^e(\mathbf{r}) + \mathbf{F}^m(\mathbf{r}) + \mathbf{F}^{em}(\mathbf{r})$  along the horizontal  $x$ -axis:  $F_x$ , and its vertical component:  $F_z$ , exerted on the cylinder.  $\lambda$  is the incident wavelength in air. The two peaks of the numerical simulation MR for  $\lambda < 1.8\mu m$  represent multipolar modes of the cylinder and thus are not covered by the analytical calculation AR that assumes the particle scattering being given by  $a_0$  and  $a_1$  only. On the other hand, in the range  $\lambda > 1.8\mu m$ , in which the scattering is due to the induced electric and magnetic dipoles, peaked at  $\lambda_1 \simeq 1.8\mu m$  and  $\lambda_2 \simeq 2.7\mu m$ , respectively, (on comparing the AR and MR dipolar peaks in Fig. 5 [see also Fig. 3(b)] notice their red-shift due to the presence of the plane), we observe a much better agreement, even within the regions of these resonance maxima, between the analytical (AR) and the

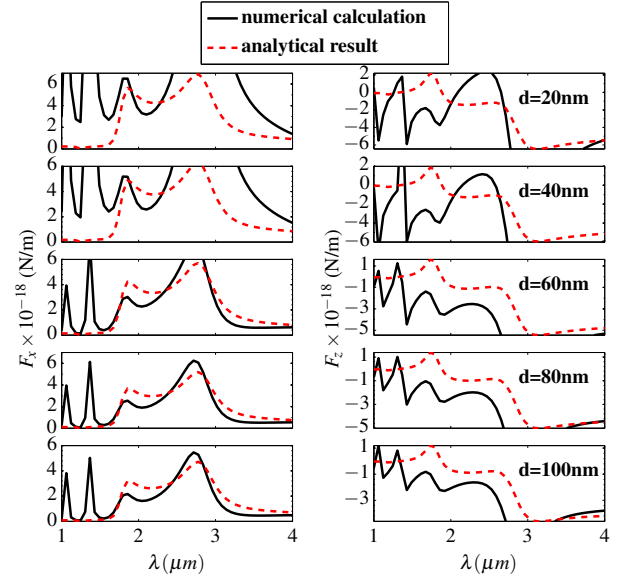


FIG. 5. Optical forces, in  $N/m$ , from a  $p$ -polarized evanescent plane wave created by TIR, on a Si cylinder ( $r_0 = 300nm$ ) in air, with its axis at distance  $d + r_0$  from a dielectric plane  $z = 0$ , (see text). Left: lateral force  $F_x$ . Right: perpendicular force  $F_z$ . The solid and dashed lines correspond to MR and AR, respectively.

full numerical (MR) calculations, providing that  $d/\lambda$  is not smaller than  $r_0/4$ .

The departure between both models is evidently larger as there is conversion by multiple scattering of a bigger proportion of evanescent waves (contributing to the gradient vertical force  $F_z$ ) into radiative components (responsible of the radiation pressure in both the  $x$  and  $z$  directions) and viceversa [15, 27, 29]). Of course as the incident wavelength grows, the dipolar response of the particle increases, the multiple reflection effect diminishes, both theoretical AR and numerical MR results tend to coincide with each other, and the gradient force  $F_z$  dominates and remains attractive towards the plane  $z = 0$ .

Notice that at any distance the radiation pressure  $F_x$  is always positive, thus NRP cannot be obtained either with or without multiple reflections [14]. However it is remarkable that the presence of multiple scattering between the particle and the plane, obviously prevailing as  $d$  decreases, turns the vertical force into pushing, thus loosing its gradient character. This latter change of the sign of  $F_z$  is also yielded by the AR in the vicinity of the electric dipole resonance, even though this is not confirmed by the MR. We also observe in Fig. 5 that at the Kerker wavelengths,  $F_x$  which follows the cylinder total scattering cross section also mediated by the plane, presents minima, or near minima. This result for  $F_x$  coincides with that for the radiation pressure exerted by an incident propagating plane wave [19]

As for  $F_z$  which follows both  $Re\alpha_e$  and  $Re\alpha_m$ , [see Fig. 3(b)], there is no minimum value in the region of the



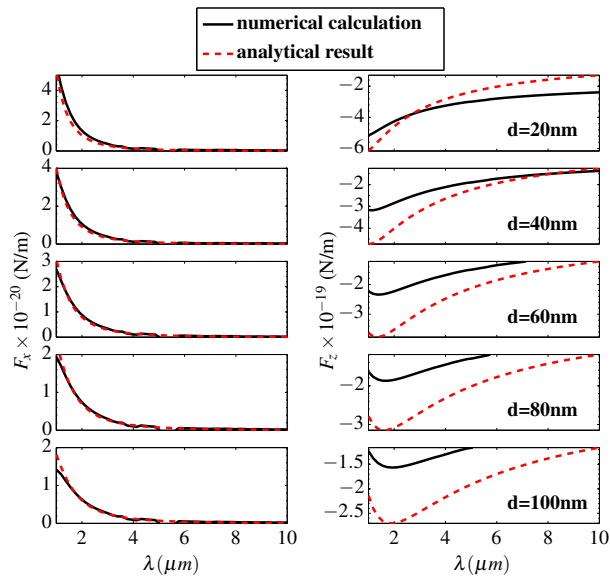


FIG. 6. The same as in Fig. 5 for a Si cylinder with  $r_0 = 50nm$ . Notice that the right column is one order of magnitude larger than the left column since in general, for small  $r_0/\lambda$ ,  $\text{Re}\alpha_e \gg \text{Im}\alpha_e$

second Kerker wavelength although there is a minimum in the neighborhood of the first Kerker condition.

Multiple reflections decrease as the particle scattering cross section diminishes. A non-resonant smaller particle, (e.g. a Si cylinder with  $r_0 = 50nm$ ), suffers negligible magnetic and electric-magnetic interference forces in the same range of  $\lambda$  as before since then  $\alpha_e \gg \alpha_m$ . This is depicted in Fig. 6. The left column exhibits a good agreement between the analytical and the numerical results. Notice that now the non-conservative component  $F_x$  is always positive, as expected, whereas  $F_z$  behaves like that of a pure pulling gradient force from an evanescent wave [15, 30]. At this point it is worth remarking that the dependence on  $\lambda$  of both  $F_x$  and  $F_z$  is proportional to  $\pm \exp[4\pi z \sqrt{(n_1 \sin \theta_0)^2 - 1}]/\lambda$ , (the signs  $+$  and  $-$  apply for  $F_x$  for  $F_z$ , respectively) [14, 15], and this exponential has a maximum (minimum) at  $\lambda = 4\pi z \sqrt{(n_1 \sin \theta_0)^2 - 1}$ . In particular, for e.g.  $d = 80nm$  the maximum (minimum) is at  $\lambda = 1.7\mu m$ . This justifies the range of wavelengths there addressed.

#### IV. CONCLUSIONS

We have demonstrated that the vertical force exerted by an evanescent Bessel beam on a magnetic resonant particle presents unusual effects, similar, and reciprocal, to those of a propagating Bessel beam. While the latter may exert a NRP, the former contrary to evanescent waves studied so far, can produce a positive force on the body, pushing it outside the plane substrate. To this effect contributes the force arising from the interference of

the electric and magnetic dipoles excited in the particle. The illumination wavelength also determines whether the system configures, or not, a trap. In any case, the strong variation of the mechanical action with the frequency, also suggests its use for sorting purposes.

To deal in 2D with the effect of interactions of the scattered waves with the plane that creates the incident evanescent field, we have presented an analysis of the Kerker conditions, (previously established for spheres), for magnetodielectric infinitely long cylinders. Showing that under  $p$ -polarization these 2D objects practically reproduce the zero or near-zero backward, as well as the near-zero forward scattered intensities.

These Kerker wavelengths are also close to those at which the magnitudes of the horizontal and vertical forces present a minimum. This work also points out the importance of multiple scatterings and their consequences on the signs of the forces for these resonant particles.

## APPENDIX: ELECTRIC AND MAGNETIC POLARIZABILITIES OF INFINITELY LONG CYLINDERS

We address the expressions for the electric and magnetic polarizabilities for infinitely long magnetodielectric cylinders in terms of the Mie coefficients. Firstly, from a general point of view, let us express the electromagnetic field scattered (in SI units) by an electric ( $\mathbf{p}$ ) and magnetic ( $\mathbf{m}$ ) dipoles placed at  $\boldsymbol{\rho}_0$  [35]

$$\begin{aligned} \mathbf{E}_s(\boldsymbol{\rho}, \boldsymbol{\rho}_0, \omega) &= \mu_0 \omega^2 \overset{\leftrightarrow p}{G}(\boldsymbol{\rho}, \boldsymbol{\rho}_0, \omega) \mathbf{p}(\boldsymbol{\rho}_0, \omega) \\ &\quad - \overset{\leftrightarrow m}{G}(\boldsymbol{\rho}, \boldsymbol{\rho}_0, \omega) \mathbf{m}(\boldsymbol{\rho}_0, \omega), \end{aligned} \quad (20)$$

where  $\overset{\leftrightarrow p, m}{G}(\boldsymbol{\rho}, \boldsymbol{\rho}_0, \omega)$  are the 2D Green's functions of the system. In free-space propagation, these Green's functions are:

$$\overset{\leftrightarrow p}{G}(\boldsymbol{\rho}, \boldsymbol{\rho}_0, \omega) = \left( \overset{\leftrightarrow}{I} + \frac{1}{k^2} \nabla \nabla \right) G_0(\boldsymbol{\rho}, \boldsymbol{\rho}_0, \omega), \quad (21)$$

$$\overset{\leftrightarrow m}{G}(\boldsymbol{\rho}, \boldsymbol{\rho}_0, \omega) = \nabla G_0(\boldsymbol{\rho}, \boldsymbol{\rho}_0, \omega) \times \overset{\leftrightarrow}{I}, \quad (22)$$

where  $G_0(\boldsymbol{\rho}, \boldsymbol{\rho}_0, \omega)$  is the 2D scalar Green's function

$$G_0(\boldsymbol{\rho}, \boldsymbol{\rho}_0, \omega) = \frac{i}{4} H_0(kr), \quad (23)$$

with  $r = |\boldsymbol{\rho} - \boldsymbol{\rho}_0|$  and  $H_0(kr) = H_0^{(1)}(kr)$  denotes the first Hankel function. The main goal is to compare Eq. (20) with the scattered electromagnetic field obtained from the Mie scattering theory.

### 1. S-polarization

Let us consider an incident electromagnetic field impinging in an infinitely long cylinder of radius  $r_0$  and refractive index  $n_p = \sqrt{\varepsilon_p \mu_p}$  immersed in vacuum, the electric vector being parallel to the cylinder axis, i.e.,  $\mathbf{E}_{in} = E_0 e^{ikx} \hat{\mathbf{u}}_z$  ( $k = \omega/c = 2\pi/\lambda$ ). For this polarization, the induced electric and magnetic dipoles at the position of the particle are

$$\mathbf{p}(0, \omega) = \varepsilon_0 \alpha_e^s E_0 \hat{\mathbf{u}}_z, \quad (24)$$

$$\mathbf{m}(0, \omega) = \alpha_m^s H_0 \hat{\mathbf{u}}_y, \quad (25)$$

where  $\alpha_e^s, \alpha_m^s$  read [36–39]

$$\alpha_e^s = \frac{\alpha_{e,0}^s}{1 - \frac{ik^2 \alpha_0^s}{4}} \quad (26)$$

$$\alpha_m^s = \frac{\alpha_{m,0}^s}{1 - \frac{i\alpha_{m,0}^s k^2}{8}}, \quad (27)$$

In the Rayleigh limit  $kn_p r_0 \ll 1$ , the static polarizabilities are  $\alpha_{e,0}^s = \pi r_0^2 (\varepsilon_p - 1)$ ,  $\alpha_{m,0}^s = 2\pi r_0^2 \frac{\mu_p - 1}{\mu_p + 1}$ . The superscript  $s$  is understood as  $s$ -polarization.

On the other hand, from Mie theory the scattered field from a infinite right circular cylinder is [28]

$$\begin{aligned} \mathbf{E}_s(\boldsymbol{\rho}, \boldsymbol{\rho}_0, \omega) &= \\ &-E_0 \sqrt{\frac{2}{\pi k r}} e^{-i\pi/4} e^{ikr} \left[ b_0 + 2 \sum_{n=1}^{\infty} b_n \cos(n(\pi - \phi)) \right] \mathbf{u}_z, \end{aligned} \quad (28)$$

where  $b_n$  are the well-known Mie coefficients and  $\phi$  is the angle defined between the scattering direction and the  $x$ -axis.

Substituting Eqs. (24) and (25) into Eq. (20), the scattered field can be expressed in terms of the electric and magnetic polarizabilities, i.e.,

$$\begin{aligned} \mathbf{E}_s &= E_0 \frac{k^2}{4} [i\alpha_e^s H_0(kr) + \alpha_m^s H_1(kr) \cos \phi] \hat{\mathbf{u}}_z \\ &= E_0 \sqrt{\frac{2}{\pi k r}} e^{-i\pi/4} e^{ikr} \frac{ik^2}{4} [\alpha_e^s - \alpha_m^s \cos \phi] \hat{\mathbf{u}}_z \end{aligned} \quad (29)$$

$H_n$  are now the Hankel functions of the first kind, that in far-field  $kr \gg 1$  read:  $H_n(kr) \sim \sqrt{\frac{2}{\pi k r}} e^{ikr} (-i)^n e^{-i\pi/4}$ .

Comparing Eqs. (29) and (28), we obtain, for  $s$ -polarization, the electric and magnetic polarizabilities in terms of the two first Mie coefficient  $b_0$  and  $b_1$ :

$$\alpha_e^s = i \frac{4}{k^2} b_0, \quad \alpha_m^s = i \frac{8}{k^2} b_1 \quad (30)$$

It is worth remarking that these expressions characterize a dipolar cylinder in the wide sense, i.e. beyond the aforementioned Rayleigh limit of small particle as they are valid whenever the scattering cross section of the cylinder is fully characterized by  $b_0$  and  $b_1$ . Notice also that the magnetic polarizability  $\alpha_m^s$  of (30) corrects by a factor 2 that given in reference [18].

We emphasize that these electric and magnetic polarizabilities are expressed in the form of Eqs. (26)-(27) with their static values being:

$$\alpha_{e,0}^s = \frac{4}{k^2} \frac{J_0(mx) J_0'(x) - m J_0'(mx) J_0(x)}{J_0(mx) Y_0'(x) - m J_0'(mx) Y_0(x)}, \quad (31)$$

$$\alpha_{m,0}^s = \frac{8}{k^2} \frac{J_1(mx) J_1'(x) - m J_1'(mx) J_1(x)}{J_1(mx) Y_1'(x) - m J_1'(mx) Y_1(x)} \quad (32)$$

where  $m = n_p$ , and  $J_n(x)$  and  $Y_n(x)$  are the Bessel functions of the first and second kind respectively.

### 2. P-polarization

Let us now consider the magnetic field polarized along the cylinder axis, i.e.,  $\mathbf{H}_{in} = H_0 e^{ikx} \hat{\mathbf{u}}_z$ . For this polarization, the induced electric and magnetic dipoles can be expressed

$$\mathbf{p}(0, \omega) = \varepsilon_0 \alpha_e^p E_0 \hat{\mathbf{u}}_y, \quad (33)$$

$$\mathbf{m}(0, \omega) = \alpha_m^p H_0 \hat{\mathbf{u}}_z, \quad (34)$$



where  $\alpha_{e,m}^p$  are the expressions for the dynamic polarizabilities [36–39]

$$\alpha_e^p = \frac{\alpha_{e,0}^p}{1 - \frac{ik^2 \alpha_{e,0}^p}{8}}, \quad (35)$$

$$\alpha_m^p = \frac{\alpha_{m,0}^p}{1 - \frac{i\alpha_{m,0}^p k^2}{4}}, \quad (36)$$

In the Rayleigh limit  $\alpha_{e,0}^p = 2\pi r_0^2 \frac{\varepsilon_p - 1}{\varepsilon_p + 1}$ ,  $\alpha_{m,0}^p = \pi r_0^2 (\mu_p - 1)$ .

On the other hand, analogously to the previous subsection, the scattered field in terms of the Mie coefficients  $a_n$  is

$$\mathbf{H}_s(\boldsymbol{\rho}, \boldsymbol{\rho}_0, \omega) = -H_0 \sqrt{\frac{2}{\pi k r}} e^{-i\pi/4} e^{ikr} \left[ a_0 + 2 \sum_{n=1}^{\infty} a_n \cos(n(\pi - \phi)) \right] \hat{\mathbf{u}}_z, \quad (37)$$

Using the Green function we obtain for the scattered field

in terms of the dynamic polarizabilities:

$$\begin{aligned} \mathbf{H}_s &= H_0 \frac{k^2}{4} [i\alpha_m^p H_0(kr) + \alpha_e^p H_1(kr) \cos \phi] \hat{\mathbf{u}}_z \\ &= H_0 \sqrt{\frac{2}{\pi k r}} e^{-i\pi/4} e^{ikr} \frac{ik^2}{4} [\alpha_m^p - \alpha_e^s \cos \phi] \hat{\mathbf{u}}_z. \end{aligned} \quad (38)$$

From this latter expression and Eq. (37) we write, for  $p$ -polarization, the electric and magnetic polarizabilities in terms of the two first Mie coefficients  $a_0$  and  $a_1$

$$\alpha_e^p = i \frac{8}{k^2} a_1, \quad \alpha_m^p = i \frac{4}{k^2} a_0 \quad (39)$$

To obtain the expression of the polarizabilities in Gaussian units, sometimes used in the literature, one must divide Eq. (39) by  $4\pi$ , (see also Eq. (18) of the main text). In addition, one can also write the polarizabilities using Eqs. (35)-(36) with the static values

$$\alpha_{e,0}^p = \frac{8}{k^2} \frac{m J_1'(x) J_1(mx) - J_1(x) J_1'(mx)}{m J_1(mx) Y_1'(x) - J_1'(mx) Y_1(x)} \quad (40)$$

$$\alpha_{m,0}^p = \frac{4}{k^2} \frac{m J_0'(x) J_0(mx) - J_0(x) J_0'(mx)}{m J_0(mx) Y_0'(x) - J_0'(mx) Y_0(x)} \quad (41)$$

## ACKNOWLEDGMENTS

Work supported by the Spanish Ministerio de Economía y Competitividad (MINECO) through FIS2012-36113-C03-03 research grant. JMA acknowledges a MINECO fellowship. We thank an anonymous reviewer for valuable comments.

- 
- [1] S. Kawata and T. Sugiura, “Movement of micrometer-sized particles in the evanescent field of a laser beam,” *Opt. Lett.* **17**, 772–774 (1992).
  - [2] E. Almaas and I. Brevik, “Radiation forces on a micrometer-sized sphere in an evanescent field,” *J. Opt. Soc. Am. B* **12**, 2429–2438 (1995).
  - [3] J. R. Arias-González, M. Nieto-Vesperinas, and M. Lester, “Modeling photonic force microscopy with metallic particles under plasmon eigenmode excitation,” *Phys. Rev. B* **65**, 115402 (2002).
  - [4] P. C. Chaumet, A. Rahmani, and M. Nieto-Vesperinas, “Optical trapping and manipulation of nano-objects with an apertureless probe,” *Phys. Rev. Lett.* **88**, 123601 (2002).
  - [5] A. S. Zelenina, R. Quidant, and M. Nieto-Vesperinas, “Enhanced optical forces between coupled resonant metal nanoparticles,” *Opt. Lett.* **32**, 1156–1158 (2007).
  - [6] G. Volpe, R. Quidant, G. Badenes, and D. Petrov, “Surface plasmon radiation forces,” *Phys. Rev. Lett.* **96**, 238101 (2006).
  - [7] J. Chen, J. Ng, Z. Lin, and C. T. Chan, “Optical pulling force,” *Nature Photon.* **5**, 531–534 (2011).
  - [8] A. Novitsky, C. W. Qiu, and H. Wang, “Single Gradientless Light Beam Drags Particles as Tractor Beams,” *Phys. Rev. Lett.* **107**, 203601 (2011).
  - [9] S. Sukhov and A. Dogariu, “Negative nonconservative forces: optical ‘tractor beams’ for arbitrary objects,” *Phys. Rev. Lett.* **107**, 203602 (2011).
  - [10] A. Novitsky, C.-W. Qiu, and A. Lavrinenko, “Material-independent and size-independent tractor beams for dipole objects,” *Phys. Rev. Lett.* **109**, 023902 (2012).
  - [11] M. Nieto-Vesperinas, J. J. Sáenz, R. Gómez-Medina, and L. Chantada, “Optical forces on small magnetodielectric particles,” *Opt. Express* **18**, 11428–11443 (2010).
  - [12] A. García-Etxarri, R. Gómez-Medina, L. S. Froufe-Pérez, C. López, L. Chantada, F. Scheffold, J. Aizpurua, M. Nieto-Vesperinas, and J. J. Sáenz, “Strong magnetic response of submicron Silicon particles in the infrared,” *Opt. Express* **19**, 4815–4826 (2011).

- [13] D. G. Grier, “A revolution in optical manipulation,” *Nature* **424**, 810–816 (2003).
- [14] M. Nieto-Vesperinas and J. J. Sáenz, “Optical forces from an evanescent wave on a magnetodielectric small particle,” *Opt. Lett.* **35**, 4078–4080 (2010).
- [15] J. R. Arias-González and M. Nieto-Vesperinas, “Optical forces on small particles: attractive and repulsive nature and plasmon-resonance conditions,” *J. Opt. Soc. Am. A* **20**, 1201–1209 (2003).
- [16] W.-P. Zang, Y. Yang, Z.-Y. Zhao, and J.-G. Tian, “The effects of multiple scattering to optical forces on a sphere in an evanescent field,” *Opt. Express* **21**, 12373–12384 (2013).
- [17] L. Peng, L. Ran, H. Chen, H. Zhang, J. A. Kong, and T. M. Grzegorzczk, “Experimental observation of left-handed behavior in an array of standard dielectric resonators,” *Phys. Rev. Lett.* **98**, 157403 (2007).
- [18] K. Vynck, D. Felbacq, E. Centeno, A. I. Căbuz, D. Casagne, and B. Guizal, “All-dielectric rod-type metamaterials at optical frequencies,” *Phys. Rev. Lett.* **102**, 133901 (2009).
- [19] M. Nieto-Vesperinas, R. Gomez-Medina, and J. J. Sáenz, “Angle-suppressed scattering and optical forces on sub-micrometer dielectric particles,” *J. Opt. Soc. Am. A* **28**, 54–60 (2011).
- [20] J. Geffrin, B. García-Cámara, R. Gómez-Medina, P. Albella, L. Froufe-Pérez, C. Eyraud, A. Litman, R. Vailion, F. González, M. Nieto-Vesperinas, J. Sáenz, and F. Moreno, “Magnetic and electric coherence in forward- and back-scattered electromagnetic waves by a single dielectric subwavelength sphere,” *Nature Communications* **3**, 1171– (2012).
- [21] D. S. Filonov, A. E. Krasnok, A. P. Slobozhanyuk, P. V. Kapitanova, E. A. Nenasheva, Y. S. Kivshar, and P. A. Belov, “Experimental verification of the concept of all-dielectric nanoantennas,” *Applied Physics Letters* **100**, 201113 (2012).
- [22] J. Durnin, J. J. Miceli, and J. H. Eberly, “Diffraction-free beams,” *Phys. Rev. Lett.* **58**, 1499–1501 (1987).
- [23] J. Durnin, “Exact solutions for nondiffracting beams. i. the scalar theory,” *J. Opt. Soc. Am. A* **4**, 651–654 (1987).
- [24] M. Kerker, D.-S. Wang, and C. L. Giles, “Electromagnetic scattering by magnetic spheres,” *J. Opt. Soc. Am.* **73**, 765–767 (1983).
- [25] A. V. Novitsky and L. M. Barkovsky, “Total internal reflection of vector bessel beams: Imbertfedorov shift and intensity transformation,” *Journal of Optics A: Pure and Applied Optics* **10**, 075006 (2008).
- [26] S. Ruschin and A. Leizer, “Evanescent bessel beams,” *J. Opt. Soc. Am. A* **15**, 1139–1143 (1998).
- [27] J. M. Auñón, C. W. Qiu, and M. Nieto-Vesperinas, “Tailoring photonic forces on a magnetodielectric nanoparticle with a fluctuating optical source,” *Phys. Rev. A* **88**, 043817 (2013).
- [28] C. F. Bohren and D. R. Huffman, *Absorption and scattering of light by small particles* (Wiley, 1983).
- [29] J. M. Auñón and M. Nieto-Vesperinas, “Photonic forces in the near field of statistically homogeneous fluctuating sources,” *Phys. Rev. A* **85**, 053828 (2012).
- [30] P. C. Chaumet and M. Nieto-Vesperinas, “Electromagnetic force on a metallic particle in the presence of a dielectric surface,” *Phys. Rev. B* **62**, 11185–11191 (2000).
- [31] M. Nieto-Vesperinas, *Scattering and Diffraction in Physical Optics* (World Science, Singapur, 2006).
- [32] L. Mandel and E. Wolf, *Optical Coherence and Quantum Optics* (Cambridge U. Press, Cambridge, UK, 1995).
- [33] J. D. Jackson, *Classical Electrodynamics* (Wiley, New York, New York, 1998).
- [34] F. J. Valdivia-Valero and M. Nieto-Vesperinas, “Optical forces on cylinders near subwavelength slits: effects of extraordinary transmission and excitation of mie resonances,” *Opt. Express* **20**, 13368–13389 (2012).
- [35] A. Yaghjian, “Electric dyadic green’s functions in the source region,” *Proceedings of the IEEE* **68**, 248–263 (1980).
- [36] A. Lakhtakia, “Strong and weak forms of the method of moments and the coupled dipole method for scattering of time-harmonic electromagnetic fields,” *International Journal of Modern Physics C* **03**, 583–603 (1992).
- [37] A. Madrazo, M. NietoVesperinas and N. Garcia, “Exact calculation of Maxwell equations for a tip-metallic interface configuration: Application to atomic resolution by photon emission,” *Phys. Rev. B* **53**, 3654–3657 (1996).
- [38] A. Garcia-Martin, J.A. Torres, J.J. Saenz y M. Nieto-Vesperinas, “Intensity Distribution of Transmitted Waves in Surface Corrugated Waveguides,” *Phys. Rev. Lett.* **80**, 4165–4168 (1998).
- [39] P. C. Chaumet and M. Nieto-Vesperinas, “Coupled dipole method determination of the electromagnetic force on a particle over a flat dielectric substrate,” *Phys. Rev. B* **61**, 14119–14127 (2000).